Engineering 3 (2017)

Contents lists available at ScienceDirect

Engineering

journal homepage: www.elsevier.com/locate/eng

Supplementary Information for

Improved Oxygen Evolution Kinetics and Surface States Passivation of Ni-B_i Co-Catalyst for a Hematite Photoanode

Ke Dang [a,b], Tuo Wang [a,b], Chengcheng Li [a,b], Jijie Zhang [a,b], Shanshan Liu [a,b], Jinlong Gong [a,b,*]

[a] Key Laboratory for Green Chemical Technology of Ministry of Education, School of Chemical Engineering and Technology, Tianjin University, Tianjin 300072, China
[b] Collaborative Innovation Center of Chemical Science and Engineering, Tianjin 300072, China

Experimental section

1. Materials

Nickel(II) nitrate hexahydrate ($Ni(NO_3)_2{\cdot}6H_2O$, > 98%), boric acid (H_3BO_3, ≥ 99.5%), iron(III) chloride hexahydrate ($FeCl_3{\cdot}6H_2O$, ≥ 99.5%), potassium hydroxide (KOH, ≥ 99.5%), hydrochloric acid (HCl, GR), and hydrogen peroxide (H_2O_2, GR) were used as received from Tianjin Kemi'ou Reagent Co., Ltd. Sodium nitrate ($NaNO_3$, 98%) was supplied by Alfa Aesar Chemical Co., Ltd. High-purity water (18.25 MΩ·cm) supplied by a UP Water Purification System was used for all experimental processes. All the reagents were used without any purification process. Fluorine-doped tin oxide (FTO) substrates (F∶SnO_2, 14 Ω·square^{-1}) were purchased from Nippon Sheet Glass, Japan. Before using, the FTO substrates were ultrasonically cleaned for 30 min each in acetone, ethanol, and deionized water, respectively.

2. Preparation of hematite photoanode

The hematite (Fe_2O_3) photoanode was prepared using a previously reported hydrothermal approach [1]. The experiment was performed with reagent-grade chemicals in an aqueous solution containing 0.15 mol·L^{-1} $FeCl_3{\cdot}6H_2O$ and 1 mol·L^{-1} $NaNO_3$ at pH 1.5 (set by HCl) in a beaker. The FTO substrate was cut into small pieces (1 × 5 cm^2) and cleaned with ethanol before using. The solution was then transferred into a Teflon-lined autoclave reactor, where a piece of FTO glass was placed with its conductive face down. The hydrothermal reaction was conducted at 95 °C for 10 h. After the reaction, the autoclave was cooled down to room temperature naturally. The obtained FeOOH electrode was cleaned with water and dried at 80 °C. Afterwards, the electrode was annealed at 800 °C for 10 min to obtain the Fe_2O_3 photoanode.

3. Ni-B_i co-catalyst electrodeposition and anodization

The Ni-B_i film was prepared on the Fe_2O_3 electrode by means of a modification of the electrodeposition methods previously reported by Dincă et al. [2]. The electrolyte was a 0.1 mol·L^{-1} potassium borate (KB_i, pH 9.2) solution containing 0.4 mmol·L^{-1} Ni^{2+}. To minimize the precipitation of $Ni(OH)_2$ from the solution, 50 mL of 0.2 mol·L^{-1} KB_i was added to 50 mL of 0.8 mmol·L^{-1} Ni^{2+} solution. A strip of black insulating tape was applied to the Fe_2O_3-coated side such that a 1 cm^2 area was exposed to the solution. Electrodeposition in the prepared electrolytic bath was carried out potentiostatically in a typical three-electrode system using the Fe_2O_3 electrode as the working electrode (WE), a platinum (Pt) foil (2 × 2 cm^2) as the counter electrode (CE), and saturated Ag/AgCl as the reference electrode (RE). The potential for deposition was controlled at 1.15 V versus the saturated Ag/AgCl (vs. Ag/AgCl) electrode. A typical deposition lasted 70 s. Following deposition, the film was rinsed by dipping it briefly in 0.1 mol·L^{-1} KB_i (pH 9.2) solution to remove any adventitious Ni^{2+}.

Anodized films were subsequently electrochemically treated in 0.5 mol·L^{-1} KB_i (pH 9.2) electrolyte by controlling the potential of 1.1 V vs. Ag/AgCl. The anodization process lasted for 1 h.

4. Photodeposition/electrodeposition of NiOOH co-catalyst

NiOOH/Fe_2O_3 electrodes were synthesized through a photodeposition/electrodeposition procedure, as previously reported [3]. The Fe_2O_3 electrodes were immersed in a 0.1 mol·L^{-1} $Ni(NO_3)_2$ solution with the pH adjusted to 6.6 by adding NaOH. Prior to the photodeposition of NiOOH, the solution was purged with nitrogen gas (N_2) for 1 h. Photodeposition was carried out in a three-electrode photoelectrochemical (PEC) cell at open-circuit voltage, using a Ag/AgCl RE and a Pt foil as the CE. The photodeposition time was 1800 s. The photodeposition was followed by an electrodeposition at 1.2 V vs. Ag/AgCl for 60 s.

5. Physical characterization

The morphology and microstructure of the sample were characterized by field-emission scanning electron microscopy (SEM, Hitachi S-4800, 5 kV) with an energy-dispersive X-ray spectrum.

* Corresponding author.
E-mail address: jlgong@tju.edu.cn

http://dx.doi.org/10.1016/J.ENG.2017.03.005

Transmission electron microscopy (TEM) and high-resolution TEM images were obtained on a JEOL JEM-2100F microscope at 200 kV. Prior to the measurements, the Ni-B_i/Fe_2O_3 composites were detached from the FTO substrate and ultrasonically dispersed in ethanol, and then dipped onto a copper grid with a carbon film and dried under ambient conditions. The crystal structure was determined using an X-ray diffractometer (D/MAX-2500) with Cu Kα radiation (λ = 1.5416 Å) at 40 kV and 140 mA. The X-ray diffraction (XRD) spectra were collected over a 2θ range of 10°–90° at a scanning speed of 5°·min^{-1}. The X-ray photoelectron spectroscopy (XPS) analysis of the photoanodes was carried out on a Physical Electronics PHI 1600 ESCA system using an Al Kα X-ray source (E = 1486.6 eV). The light absorption of the as-prepared samples was obtained using a Shimadzu UV-2550 spectrophotometer equipped with an integrating sphere using $BaSO_4$ as the reflectance standard. The photoluminescence spectra were obtained using a Hitachi F-4600 fluorescence spectrophotometer with an excitation of 350 nm wavelength incident-light at ambient temperature. The composition of the as-prepared sample was measured using Agilent 7700X inductively coupled plasma mass spectrometry (ICP-MS). The film with an area of 1 cm^2 was dissolved in 5 mL HCl solution before ICP-MS measurement.

6. Photoelectrochemical measurement

PEC measurement was performed with an electrochemical workstation (IVIUM CompactStat.e20250). A three-electrode configuration was used, with the Fe_2O_3 or Ni-B_i/Fe_2O_3 electrode as the WE, a Pt foil (2 × 2 cm^2) as the CE, and the saturated Ag/AgCl as the RE. A 300 W Xenon arc lamp (Beijing Perfectlight Technology Co., Ltd., 300 UV) equipped with an air mass 1.5 global (AM 1.5G) filter was used as the light source. Unless otherwise noted, all tests were performed under front-side illumination with an illumination area of 1 cm^2, immersed in the 0.5 mol·L^{-1} KB_i buffer solution electrolyte (pH 9.2). The KB_i (pH 9.2) buffer solution was regarded as the electrolyte in order to maintain the structure of the Ni-B_i. Electrolytes with a pH close to neutral had a certain significance in the application of the PEC system because the pH of seawater varies from 7.7 to 8.4 [4]. Prior to measurements, the electrolyte was thoroughly saturated with N_2 for 0.5 h. The long-term amperometric photocurrent density-time curves were measured under continuous irradiation and at a bias of 1.23 V versus reversible hydrogen electrode (vs. RHE). The electrochemical impedance spectra (EIS) were carried out in the range of 0.01 Hz to 100 kHz, with an AC voltage amplitude of 10 mV and a DC bias of 1.5 V vs. RHE under sunlight irradiation (AM 1.5G, 100 mW·cm^{-2}) or under darkness. The Mott-Schottky plots were measured at a frequency of 1000 Hz and an amplitude of 10 mV under darkness. The incident-photo-to-current efficiency (IPCE) tests were performed as the function of wavelength from 380 nm to 650 nm at a bias of 1.23 V vs. RHE. For the photovoltage measurement, each dark/light open-circuit potential reading was obtained after a stabilization process (20–30 min) with constant stirring. The stabilization process was necessary for reproducible open-circuit potential reading. The measured potentials vs. saturated Ag/AgCl were converted to the RHE scales according to the Nernst equation: E (vs. RHE) = E (vs. Ag/AgCl) + 0.0592 × pH + 0.197. The onset potential of the photocurrent is defined as the corresponding voltage when the photocurrent density reaches 20 μA·cm^{-2} in the current-voltage measurement.

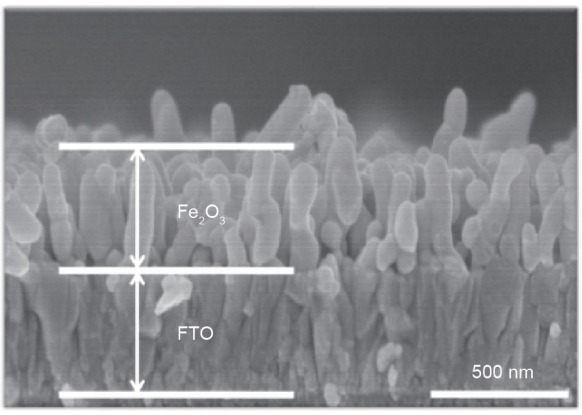

Fig. S1. Cross-sectional SEM of the Fe_2O_3 photoanode.

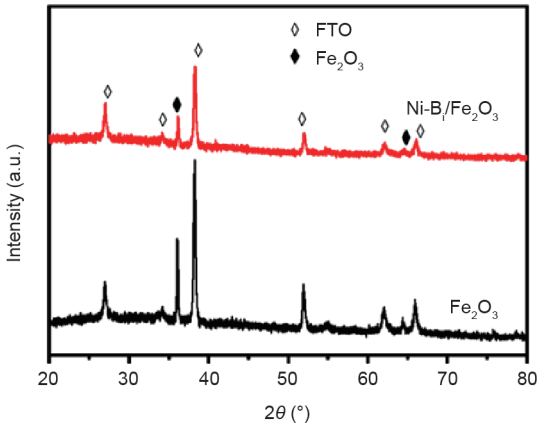

Fig. S2. XRD patterns of Fe_2O_3 and Ni-B_i/Fe_2O_3.

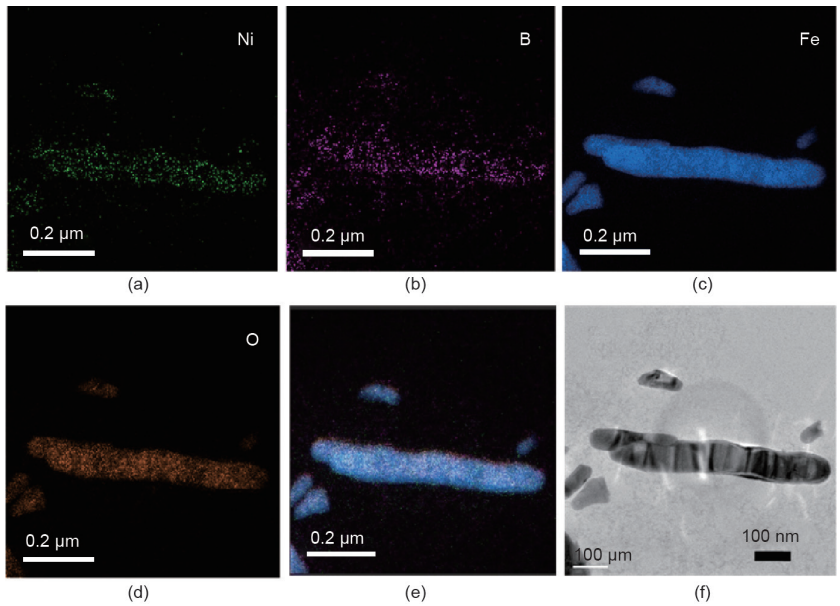

Fig. S3. Electron energy-loss spectroscopy mapping for (a) Ni, (b) B, (c) Fe, (d) elemental O, and (e) the overlap of these signals; (f) the TEM image of the selected area.

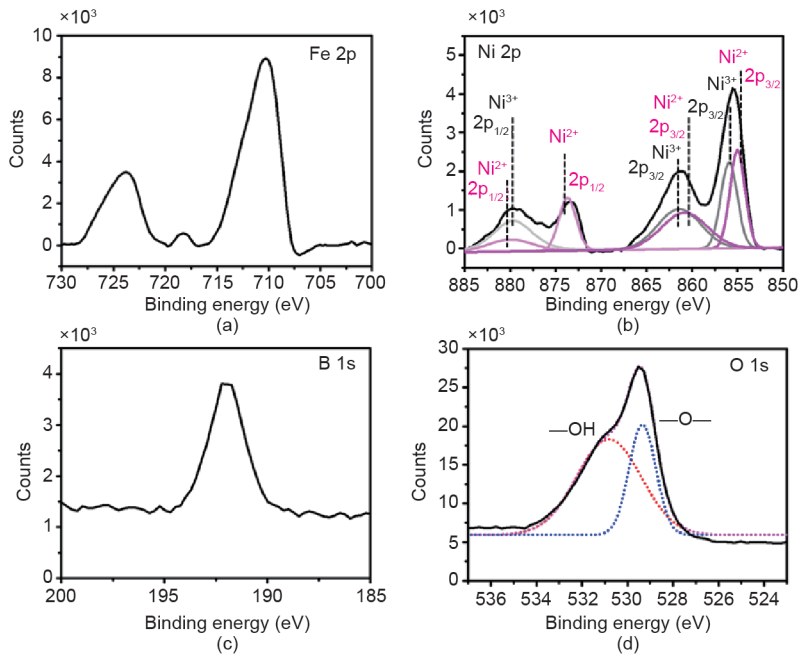

Fig. S4. XPS spectra of Ni-B_i/Fe_2O_3 for (a) Fe 2p, (b) Ni 2p, (c) B 1s, and (d) O 1s. The peaks of Ni $2p_{3/2}$ and Ni $2p_{1/2}$ located at 856.3 eV and 873.9 eV (Fig. S4(b)) illustrate the existence of Ni^{2+} and Ni^{3+} species [5]. The B peak at ~191.6 eV (Fig. S4(c)) indicates that B exists mainly in an oxidized state [6]. The peaks at 723.9 eV and 710.6 eV in the Fe 2p spectra represent the Fe $2p_{1/2}$ and Fe $2p_{3/2}$ spin-orbits in Fe_2O_3, respectively (Fig. S4(a)) [1]. A peak at 529.0 eV of the O 1s spectra corresponds to the lattice oxygen of Fe_2O_3 (Fig. S4(d)). A satellite peak found at ~531.0 eV represents the —OH species on the surface of the Ni-B_i/Fe_2O_3 photoanode, indicating the existence of the NiOOH species in the Ni-B_i (Fig. S4(d)) [7].

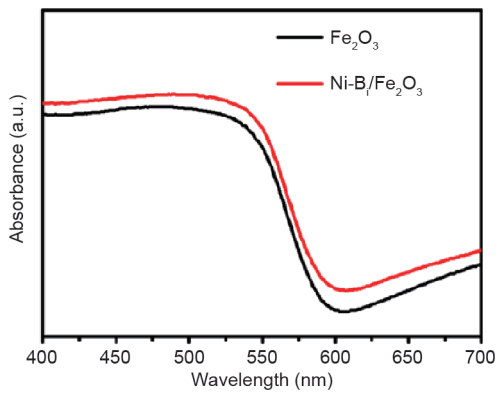

Fig. S5. The UV/visible light absorbance of Fe_2O_3 and Ni-B_i/Fe_2O_3.

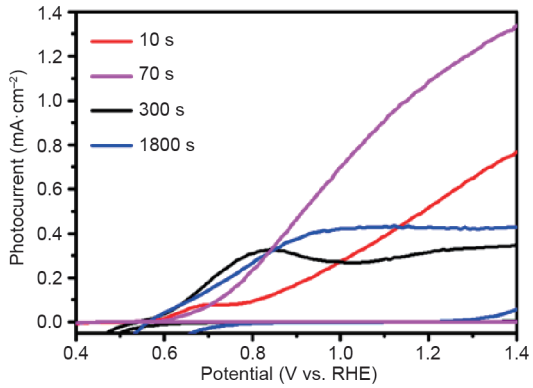

Fig. S6. Optimizations on the amount of Ni-B_i by different electrodeposition time.

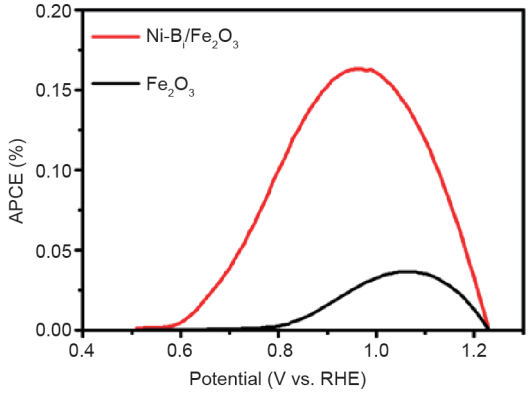

Fig. S7. Applied-bias photo-to-current conversion efficiency of Fe_2O_3 and Ni-B_i/Fe_2O_3, measured in a 0.5 mol·L^{-1} KB_i (pH 9.2) aqueous electrolyte under AM 1.5G illumination.

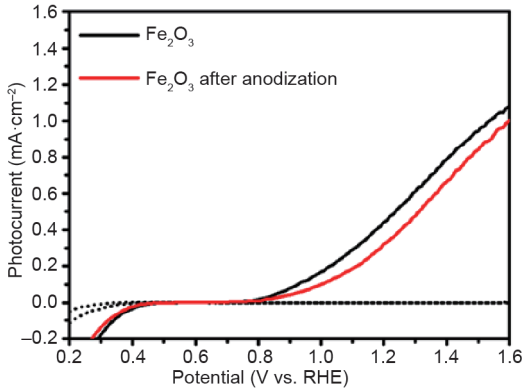

Fig. S8. Photocurrent density versus applied potential (J-V) curves of Fe_2O_3 before and after anodization. The experimental details of anodization are available in the Experimental section.

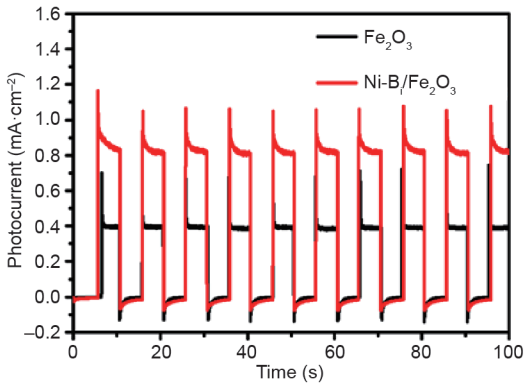

Fig. S9. Amperometric transient photocurrent curves plotted at 1.23 V vs. RHE under chopped AM 1.5G illumination. Because of the poor water oxidation kinetics of Fe_2O_3, the photogenerated holes accumulate on the surface of the photoanode, as indicated by the large transient photocurrent spikes with switching illumination. The loading of Ni-B_i reduces the amount of accumulated holes, as evidenced by the less-pronounced transient spikes.

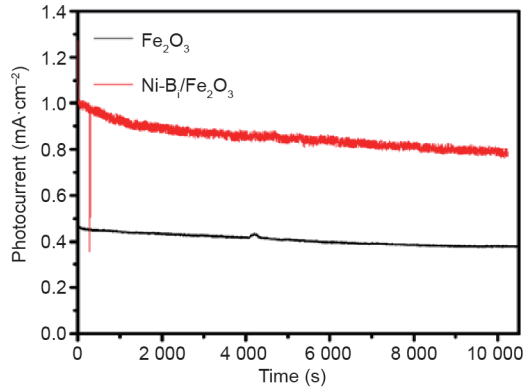

Fig. S10. Time dependence of the photocurrent density of Ni-B_i/Fe_2O_3 and Fe_2O_3 photoanodes, measured at 1.23 V vs. RHE in 0.5 mol·L^{-1} KB_i (pH 9.2) under continuous AM 1.5G simulated solar irradiation. The electrolyte was not stirred. The photocurrent of the bare Fe_2O_3 photoanode decreases by 23% during the 3 h period, while the sample coated with Ni-B_i decreases by 22% after 3 h.

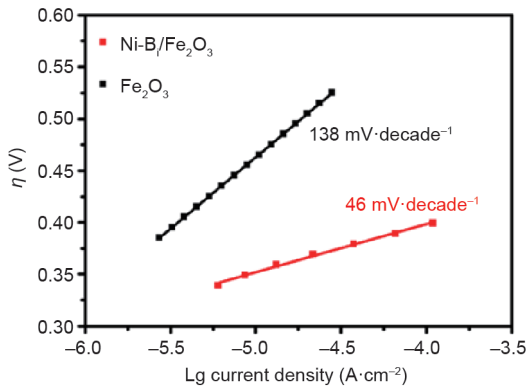

Fig. S11. The Tafel plot, $\eta = V_{appl} - E_0$, of Fe_2O_3 and Ni-B_i/Fe_2O_3 electrodes operated in 0.5 mol·L^{-1} KB_i (pH 9.2), where η is the overpotential, V_{appl} is the applied bias, and E_0 is the thermodynamic potential for water oxidation (1.23 V vs. RHE).

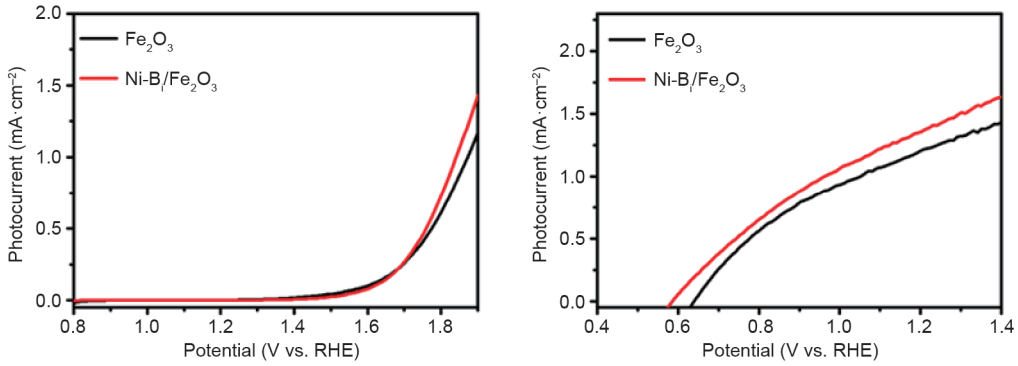

Fig. S12. J-V curves of different photoanodes measured in 0.5 mol·L^{-1} KB_i (pH 9.2) electrolyte with 0.5 mol·L^{-1} H_2O_2 as the sacrificial agent (a) in darkness and (b) under continuous AM 1.5G simulated solar irradiation.

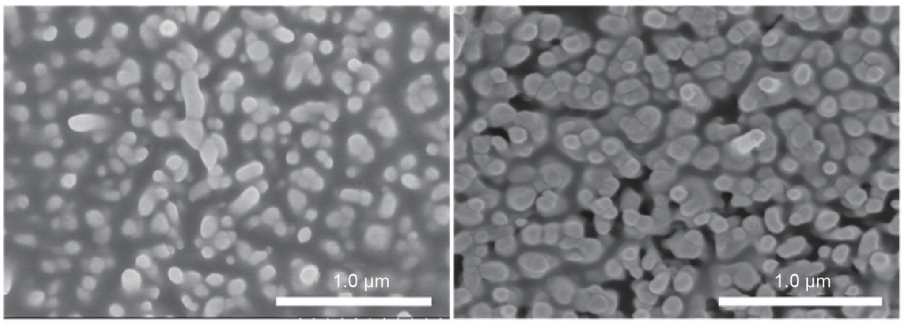

Fig. S13. SEM images of (a) Ni-B_i/Fe_2O_3 and (b) NiOOH/Fe_2O_3.

Table S1. EIS-fitting results of R_s, R_{trap}, and R_{ct} for Fe_2O_3 and Ni-B_i/Fe_2O_3 photoanodes.*

Sample	Fe_2O_3	Ni-B_i/Fe_2O_3
R_s (Ω)	86.2 ± 0.5	83.3 ± 0.7
R_{trap} (Ω)	128.1 ± 2.3	90.2 ± 2.0
R_{ct} (Ω)	321.3 ± 4.4	166.9 ± 4.2

* The equivalent circuit consists of a depletion layer capacitance (C_{bulk}), a series resistance (R_s) between Fe_2O_3 and FTO, a charge transfer resistance in bulk Fe_2O_3 (R_{trap}), a surface states trapping charge capacitance (C_{ss}), and a charge transfer resistance at the electrode/electrolyte interface (R_{ct}).

References

[1] Hu X, Yu JC, Gong J, Li Q, Li G. α-Fe_2O_3 nanorings prepared by a microwave-assisted hydrothermal process and their sensing properties. Adv Mater 2007; 19(17):2324–9.
[2] Dincă M, Surendranath Y, Nocera DG. Nickel-borate oxygen-evolving catalyst that functions under benign conditions. Proc Natl Acad Sci USA 2010;107(23):10337–41.
[3] Malara F, Minguzzi A, Marelli M, Morandi S, Psaro R, Dal Santo V, et al. α-Fe_2O_3/NiOOH: An effective heterostructure for photoelectrochemical water oxidation. ACS Catal 2015;5(9):5292–300.
[4] Ohline SM, Reid MR, Husheer SLG, Currie KI, Hunter KA. Spectrophotometric determination of pH in seawater off Taiaroa Head, Otago, New Zealand: Full-spectrum modelling and prediction of *p*CO2 levels. Mar Chem 2007;107(2):143–55.
[5] Mansour AN, Melendres CA. Characterization of α-Ni(OH)$_2$ by XPS. Surf Sci Spectra 1994;3(3):255–62.
[6] He D, Zhang L, He D, Zhou G, Lin Y, Deng Z, et al. Amorphous nickel boride membrane on a platinum-nickel alloy surface for enhanced oxygen reduction reaction. Nat Commun 2016;7:12362..
[7] Risch M, Klingan K, Heidkamp J, Ehrenberg D, Chernev P, Zaharieva I, et al. Nickel-oxido structure of a water-oxidizing catalyst film. Chem Commun 2011;47(43):11912–4.